International Journal of Concrete Structures and Materials

RESEARCH

Open Access

Repairing and Strengthening of Box-Section RC Beams Reinforced by GFRP Bars Using Epoxy Injection and GFRP Strips

Ahmed A. Mahmoud[1*], Manar S. Sedeek[1], Mohamed A. Salama[1] and Ahmed N. M. Khater[1]

Abstract

Glass-fiber-reinforced polymer (GFRP) bars are widely applied due to their advantages over reinforcement steel bars. GFRP bars are the main adhesive reinforcement since they have a high strength capacity and corrosion resistance. From the literature review and due to the insufficiency of these studies concerning the repair and strengthening of box-section RC beams reinforced by GFRP bars using external GFRP strips, this study was done. This paper presents an experimental, numerical, and analytical study for strengthening box-section reinforced concrete RC beams reinforced by GFRP bars and stirrups using external GFRP strips. The studied parameters in this investigation are (1) the width of GFRP strips (S_f), (2) the centerline-to-centerline spacing of the strips (S_f) and (W_f/S_f) ratio, (3) the GFRP layers, and (4) the inclination of GFRP strips. The experimental study consists of nine specimens. The specimens are tested as simply supported RC box-section beams. All beams have dimensions of 400 * 600 * 2200 * 2000 mm (width * depth * total length * span). The nonlinear finite element program ANSYS was used to verify and validate the numerical models. Verification models have been developed. Using the measured results as crack patterns, load–deflection curves, failure modes, and failure loads, it can be concluded that, when doubling the number of GFRP layers, the failure load increased by 82%. Due to increasing the spacing between strips, the ultimate load decreased by about 9%. The ultimate load increased by about 3% when reducing the spacing between strips. The capacity of all tested beams after repair and strengthening was calculated using the Egyptian and American codes. Both codes are unconservative in some cases and conservative in others. The numerical output is unconservative compared to the experimental results.

Keywords Box-section, Reinforced concrete, GFRP bars, GFRP stirrups, GFRP strips, Strengthening, Repair, Experimental, Nonlinear finite element, Numerical analysis, ANSYS program

Journal information: ISSN 1976- 0485 / eISSN 2234-1315.

*Correspondence:
Ahmed A. Mahmoud
ahmed.ahmed@feng.bu.edu.eg; ahmed.m5882@gmail.com
[1]Civil Engineering Department, Faculty of Engineering (Shoubra), Benha University, 108 Shoubra Street, Shoubra 11691, Cairo, Egypt.

Graphical Abstract

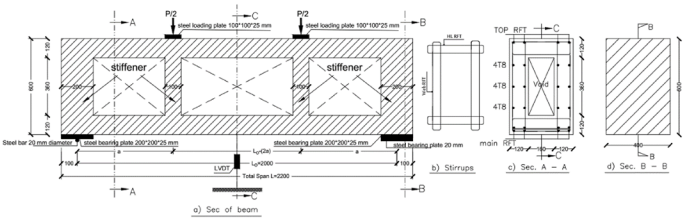

Typical dimensions and reinforcement details of specimens (mm.)

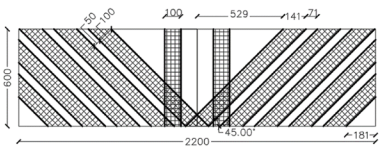

(a) Specimens $\mathbf{B_{1,1,150,100,45}}$, $\mathbf{B_{1,3,150,100,45}}$, and $\mathbf{B_{1,2,150,100,45}}$, consisting of 1, 3, and 2 layers of GFRP, respectively.

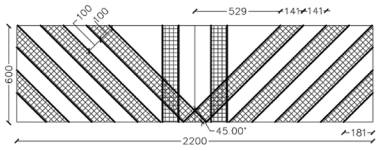

(b) Specimen $\mathbf{B_{2,1,200,100,45}}$

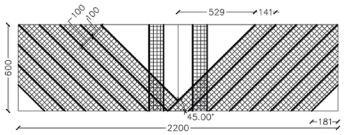

(c) Specimen $\mathbf{B_{2,1,100,100,45}}$

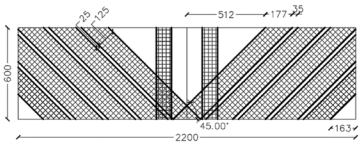

(d) Specimen $\mathbf{B_{3,1,150,125,45}}$

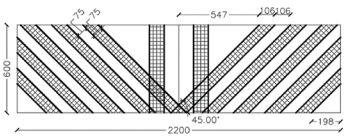

(e) Specimen $\mathbf{B_{3,1,150,75,45}}$

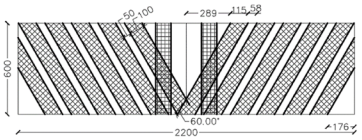

(f) Specimen $\mathbf{B_{4,1,150,100,60}}$

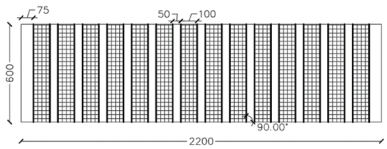

(g) Specimen $\mathbf{B_{4,1,150,100,90}}$

Details of strengthening for all tested specimens.

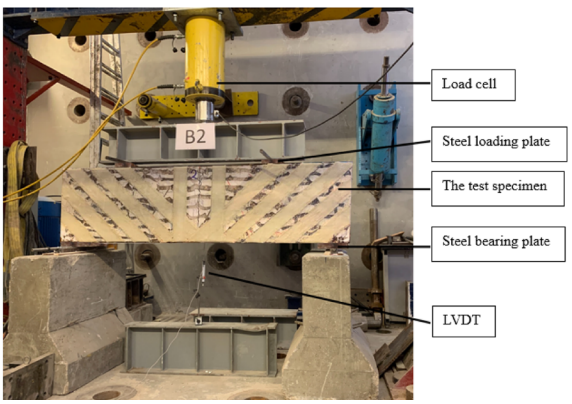

1 Introduction

The steel reinforcement bars in the concrete elements are suffering from corrosion. Reinforcement steel bars corrode faster due to severe weather. To overcome this problem, it is necessary to search for alternative reinforcement and external strengthening materials. GFRP has emerged as an alternative to reinforcement steel and as an external-strengthening material for the repair of RC elements. Their well-defined material properties, durability, high strength-to-weight and stiffness-to-weight ratios, and resistance to temperature change without softening or brittleness make FRP material superior to conventional materials in strengthening applications. The strengthening uses sheets like a thin polymer layer and fiber-reinforced polymer FRP such as glass (GFRP), basalt FRP (BFRP), carbon FRP (CFRP), and aramid FRP (AFRP).

Abdel Kareem (Abdel Kareem, 2014) investigated the performance of the NSM technique on shear resistance for RC beams. The specimens were strengthened using GFRP bars in a U-shaped shape, which gave an improvement in the load capacity when compared to the specimens strengthened with the NSM using GFRP bars in a U-shaped shape without using a cap. Abdel Kareem (Abdel Kareem, 2014) concluded that, because the distance between the GFRP rods was shortened, the specimens were repaired using the NSM approach, and GFRP rods shaped like a U with strands revealed an improvement in the ultimate load where the shear capacity increased from 59 to 85%.

Al Saawani et al. (Al Saawani et al., 2020) presented how the span-to-depth ratio affected the GFRP-repaired specimens' load capacity and mechanism of failure. At the same bending moment and debonding strain, the repaired specimens by GFRP failed due to intermediate crack debonding. Strengthening of beams with concrete cover separation (CCS) failed at the same load at different CFRP strains, which is a more brittle failure mode and compromises the efficiency of CFRP. When using the CFRP longitudinal strengthening of short beams with a shear-span/depth ratio of less than 2.50 m, the results showed that it is not possible to enhance the load capacity of the beams.

Nassif et al. (Nassif et al., 2021) investigated whether locally produced GFRP bars affected the performance of concrete deep beams. When using 1.2 μ_b of GFRP reinforcement ratio, as compared to beams reinforced with steel bars, where μ_b is the balanced reinforcement ratio of the beam, the crack widths and the mid-spans deflection were substantially reduced. For specimens that have concrete with strengths of 50 MPa and 60 MPa, respectively, the decrease in deflection ranged from 20 to 39%, accompanied by a substantial decrease in the widths of the concrete cracks. In addition, as the concrete strengths increased, the failure load increased by 3% and 4%, respectively.

Ebrahim et al. (Ebrahim et al., 2024) studied the shear strength of box-section RC beams with GFRP stirrups and GFRP bars. The findings show that carrying capacity, toughness, and displacement ductility are all reduced by 2%, 28%, and 12%, respectively, when the shear span-to-depth ratio is increased by 50%. The carrying capacity and toughness improved by 59% and 62%, respectively, with a 20% increase in the primary FRP reinforcement rebars. The failure load and toughness increased by 26% and 15%, respectively, when vertical FRP stirrups were increased by 79%, although displacement ductility only increased by less than 1%.

Nikopour and Nehdi (Nikopour & Nehdi, 2011) studied the behavior of RC beams repaired using uni-directional and bi-directional GFRP sheets subjected to cyclic loading. Hybrid application of GFRP sheets showed better performance in increasing the ultimate shear capacity of retrofitted RC beams compared with uni-directional CFR-retrofitted beam specimens. Nikopour and Nehdi (Nikopour & Nehdi, 2011) concluded that the crack injection using low-viscosity epoxy provided an increase in the stiffness in the linear region of the load–displacement curves of all repaired RC beams. In addition, fatigue and repetitive loading affect the ultimate load capacity of RC beams through the formation of micro-cracks in the concrete and the weakening of the bonding layer between the concrete and the external GFRP sheets.

Haddad et al. (Haddad et al., 2013) studied the use of advanced composite materials in repairing shear-deficient RC prototypes. Haddad et al. (Haddad et al., 2013) concluded that the beams damaged by a sulfate cyclic treatment were repaired using varying types of CFRP and GFRP sheets and strips. In addition, the efficiency of GFRP composites as repair materials for sulfate-damaged and shear-deficient beams was significantly affected by induced damage. Haddad et al. (Haddad et al., 2013) concluded that the present sulfate-damaged and repaired beams reached less failure load by about 4–30% and GFRP strain capacities by about 26–37%, compared to intact and strengthened ones.

Abdel Kareem et al. (Abdel Kareem et al., 2019) investigated the shear strengthening of RC beams with rectangular web openings. Abdel Kareem et al. (Abdel Kareem et al., 2019) concluded that the GFRP strengthening around the web openings results in a remarkable increase in stiffness, especially when the opening size is relatively large. In addition, Abdel Kareem et al. (Abdel Kareem et al., 2019) concluded that the complete wrapping of GFRP around the opening chords increases the beam stiffness more than U-shape strips.

Therefore, the stiffness of the strengthened beams is not affected by increasing the GFRP bonded around openings.

Siddika et al. (Siddika et al., 2019) investigated the strengthening of the RC beams using FRP composites. Siddika et al. (Siddika et al., 2019) concluded that deep beams strengthened by U-shape CFRP sheets and diagonal CFRP sheets, compared with the reference beam, resulted in a maximum increase in the load capacity of 106%.

Masoud and Khalaf (Masoud & Khalaf, 2020) studied the effect of utilizing CFRP laminates in strengthening box-section steel beams in both shear and flexural. Masoud and Khalaf (Masoud & Khalaf, 2020) concluded that the GFRP laminates are efficient at strengthening flanges in tension and web cracks, where the failure loads were between 86% and 91% of those of the reference beam, which is considered reasonable effectiveness. Masoud and Khalaf (Masoud & Khalaf, 2020) concluded that the stiffness of the repaired beams was about 70% of that of the reference beam, which is not as effective as in the case of the ultimate loads.

Zaher et al. (Zaher et al., 2020) studied the behavior of deep beams strengthened and repaired in shear using CFRP and GFRP sheets. Zaher et al. (Zaher et al., 2020) concluded that the diagonal CFRP sheets provided better enhancement than the vertical CFRP sheets in terms of the ultimate load. The deep beams strengthened by U-shape GFRP sheets and diagonal GFRP sheets compared with the control beams showed a maximum increase in the ultimate load of about 81%. Zaher et al. (Zaher et al., 2020) concluded that the deep beams pre-cracked and then repaired by diagonal CFRP and GFRP sheets, compared with the control beams, increased the ultimate load by about 61% and 48%, respectively, while the deep beams repaired by diagonal CFRP and GFRP sheets, compared with beams strengthened by vertical CFRP and GFRP sheets, decreased the ultimate load by about 45% and 34%, respectively.

Abtan et al. (Abtan, 2020) showed that for RC beams with GFRP bars in place of total or partial steel reinforcement bars, the flexural reinforcement did not significantly increase the specimen's failure load while reducing stiffness. Abtan et al. (Abtan, 2020) concluded that integrating CFRP full-side sheets that are externally connected and have a suitable proportion of steel to fiber is better than using steel stirrups; this collection enhances ultimate capacity by 11% (with 1% steel fiber). Abtan et al. (Abtan, 2020) found that when comparing the use of the CFRP sheets alone to the control beam of traditional steel stirrups, a strength efficiency of 71% was only achieved, where flexural failure was the most common mode of failure in the improved full-side sheet GFRP beams.

Hassan et al. (Hassan et al., 2020) studied the use of two layers of CFRP sheets in the strengthening of RC beams. Hassan et al. (Hassan et al., 2020) concluded that the use of two layers of CFRP sheets has a greater effect on increasing the load capacity of the beams with a minimum reinforcement ratio $\rho_{f\ min}$ and a balanced reinforcement ratio ρ_{fb}; for beams with these ratios, the load capacity increased by 95% and 31% for the number of CFRP layers 0 and 2, respectively. Although the beams have 1.3 μ_{fb} and 1.6 μ_{fb}, the load capacity

Table 1 Details of the tested beams before repair and strengthening

Group no.	Beam symbol before strengthening	Beam symbol after strengthening	a (mm)	(a/t)	Main longitudinal reinforcements RFT	Top longitudinal reinforcements	GFRP vl web RFT	GFRP hl web RFT	Notes
1	B1	$\mathbf{B_{1,1,150,100,45}}$	450	0.75	8Ø12	4Ø8	Ø8	Ø8	Effect of shear span
	B2	$\mathbf{B_{1,3,150,100,45}}$	600	1	8Ø12	4Ø8	Ø8	Ø8	
	B3	$\mathbf{B_{1,2,150,100,45}}$	900	1.5	8Ø12	4Ø8	Ø8	Ø8	
2	B4	$\mathbf{B_{2,1,200,100,45}}$	600	1	6Ø12	4Ø8	Ø8	Ø8	Effect of the main longitudinal RFT
	B5	$\mathbf{B_{2,1,100,100,45}}$	600	1	10Ø12	4Ø8	Ø8	Ø8	
3	B6	$\mathbf{B_{3,1,150,125,45}}$	600	1	8Ø12	4Ø8	Ø12	Ø8	Effect of the Vl. web RFT
	B7	$\mathbf{B_{3,1,150,75,45}}$	600	1	8Ø12	4Ø8	Ø10	Ø8	
4	B8	$\mathbf{B_{4,1,150,100,60}}$	600	1	8Ø12	4Ø8	Ø8	Ø12	Effect of the Hl. web RFT
	B9	$\mathbf{B_{4,1,150,100,90}}$	600	1	8Ø12	4Ø8	Ø8	Ø10	

Where: B_{GNSWA} means: G: is group number (1, 2, 3, and 4); N: is the number of used GFRP layers (1, 2, and 3); S: is the spacing between GFRP strips (center to center) (100 and 200 mm); W: is the width of the GFRP strips (75 and 125 mm.); and A: is the angle of inclination of the GFRP layer (60^0 and 90^0). (a/t): is the beam shear span to total depth ratio (0.75, 1, and 1.5). RFT: is the reinforcement. The vertical and horizontal stirrups have four branches with a spacing of 100 mm. The measured areas of the used ϕ 8, 10, and 12 mm are 40.7, 56.7, and 86.5 mm^2, respectively. The modulus of elasticity of the GFRP bars is 50 GPa. The GFRP bar surface was rough with protrusion on its surface. f_{cu} is the compressive strength of concrete (constant) of 29.21 MPa; b, t, d, and d` are the beam dimensions (width, total depth, effective depth, and concrete cover are constants = 400, 600, 580, and 20 mm, respectively). dimension of void = 160 * 360 mm. n is the number of the stirrup's branches

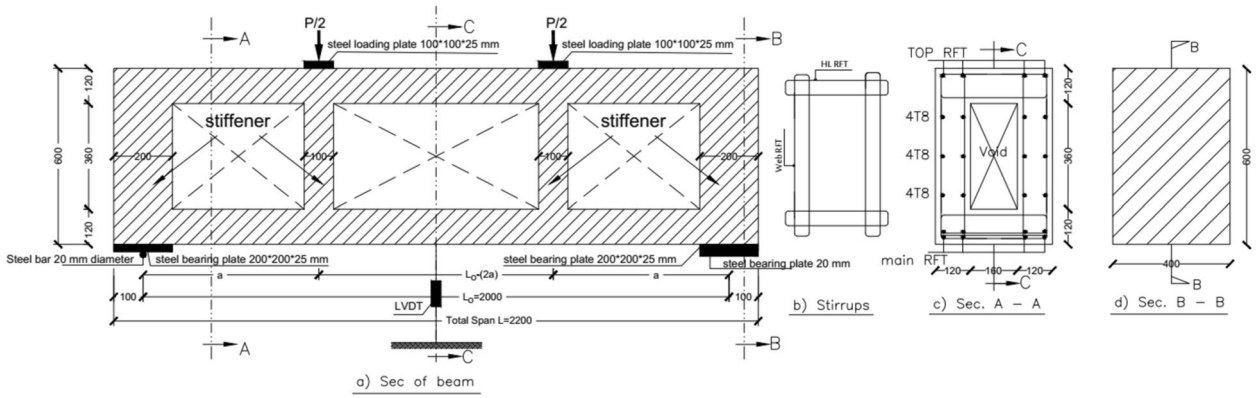

Fig. 1 Typical dimensions and reinforcement details of specimens (mm)

Table 2 Strengthening details

Group no.	Beam symbol (before/after strengthening)	Number of the used layers	S_f (mm) Spacing between strips, center to center	W_f the width of the strips (mm)	Inclination angle α (degree)	Notes
1	**B1 / $B_{1,1,150,100,45}$**	1	150	100	45	Effect of the number of layers
	B2 / $B_{1,3,150,100,45}$	3	150	100	45	
	B3 / $B_{1,2,150,100,45}$	2	150	100	45	
2	**B4 / $B_{2,1,200,100,45}$**	1	200	100	45	Effect of strip spacing
	B5 / $B_{2,1,100,100,45}$	1	100	100	45	
3	**B6 / $B_{3,1,150,125,45}$**	1	150	125	45	Effect of strip width
	B7 / $B_{3,1,150,75,45}$	1	150	75	45	
4	**B8 / $B_{4,1,150,100,60}$**	1	150	100	60	Effect of strip inclination
	B9 / $B_{4,1,150,100,90}$	1	150	100	90	

Where: S_f: is the spacing between strips and W_f: is the width of the strip

is only slightly affected by increasing the number of CFRP sheets from 1 to 2. Hassan et al. (Hassan et al., 2020) found that the failure load increased by 13% and 9% when the number of CFRP layers increased from 1 to 2 for beams with 1.3 μ_{fb} and 1.6 μ_{fb}, respectively. In addition, Hassan et al. (Hassan et al., 2020) found that when the ratio of the reinforcement is increased from $\mu_{f\,min}$ to μ_{fb}, the load capacity for beams increases by 27%.

Najaf et al. (Najaf et al., 2022) studied numerically the effect of type, number, and installation angle of FRP sheets on improving the flexural strength of concrete beams. Najaf et al. (Najaf et al., 2022) concluded that the load is increased until the compressive concrete is crushed to the point where the beam fails. In comparison to the beam with internal confinement by the inner layer, the specimen's strength and the failure load improve by 21% when prestressed GFRP sheets are added. The specimens retrofitted with CFRP material have stronger increases in strength than those retrofitted with GFRP material, and GFRP material has stronger specimens than AFRP material compared to fibers installed at a 60-degree angle; those installed at a 45-degree angle show greater efficiency. In addition, Najaf et al. (Najaf et al., 2022) concluded that the efficiency of the sheets inserted at a 60-degree angle was higher than that of the sheets installed at a 90-degree angle.

According to Huang et al. (Huang et al., 2022), the load capacity increases by 57% and 350%, respectively, when using CFRP or ultra-high-performance-concrete UHPC to strengthen RC beams. Huang et al. (Huang et al., 2022) found that with the UHPC (2% steel fiber) retrofit, the displacement increased by 652% compared to the use of CFRP. Huang et al. (Huang et al., 2022) found that an RC beam reinforced with CFRP costs two to four times as much per unit as a UHPC upgrade. In addition, Huang et al. (Huang et al., 2022) found that, as

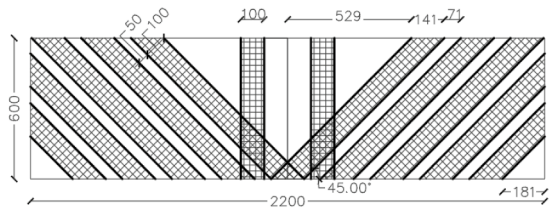

(a) Specimens $\mathbf{B_{1,1,150,100,45}}$, $\mathbf{B_{1,3,150,100,45}}$ and $\mathbf{B_{1,2,150,100,45}}$, consisting of 1, 3, and 2 layers of GFRP, respectively.

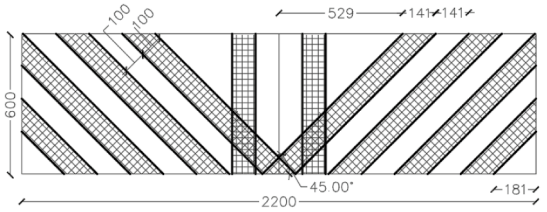

(b) Specimen $\mathbf{B_{2,1,200,100,45}}$

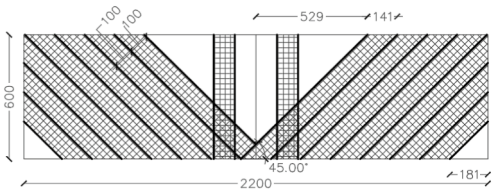

(c) Specimen $\mathbf{B_{2,1,100,100,45}}$

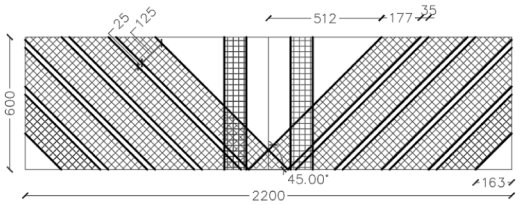

(d) Specimen $\mathbf{B_{3,1,150,125,45}}$

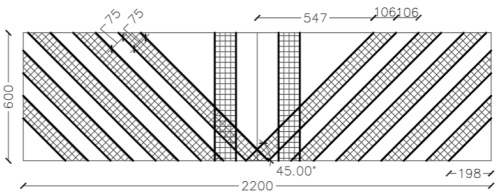

(e) Specimen $\mathbf{B_{3,1,150,75,45}}$

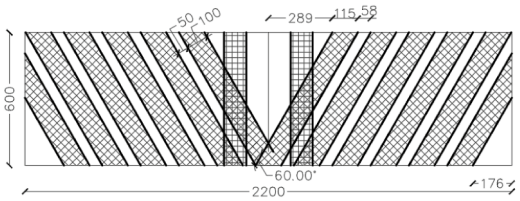

(f) Specimen $\mathbf{B_{4,1,150,100,60}}$

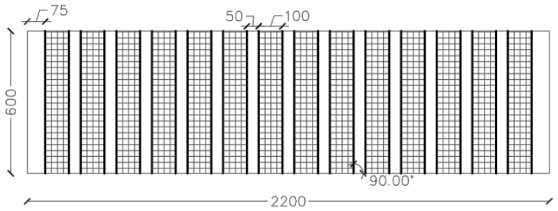

(g) Specimen $\mathbf{B_{4,1,150,100,90}}$

Fig. 2 Details of strengthening for all tested specimens

Table 3 Mechanical properties of the used strengthening materials

Type	Tensile strength (MPa)	Tensile elastic modulus (MPa)	Density (g/cm^3)	Thickness t_f (mm./ply)
GFRP sheet	2500	72,000	2.56	0.3
Kema Poxy 103	5	–	1.10	–
Kema Poxy 150	15–25	–	1.11	–
Kema Poxy 177	45	–	1.41	–

a result, compared to CFRP retrofits, UHPC has superior displacement, fracture energy, and toughness.

Muhammad et al. (Muhammad & Ahmed, 2023) studied the evaluation of the deflection and flexural performance of reinforced concrete beams with glass fiber-reinforced polymer bars. Muhammad et al. (Muhammad & Ahmed, 2023) concluded that there are three different types of failures: balanced failure, concrete crushing, and GFRP bar rupture. Muhammad et al. (Muhammad & Ahmed, 2023) found that steel yielding caused the steel reinforcing beams to fail, and as a result, the upper compressive concrete was crushed.

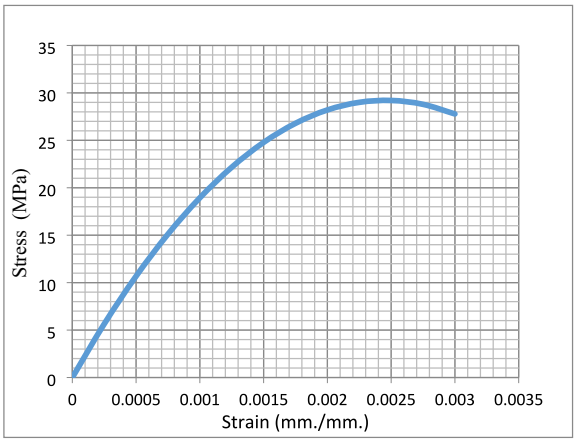

(a) Concrete compressive stress-strain curve.

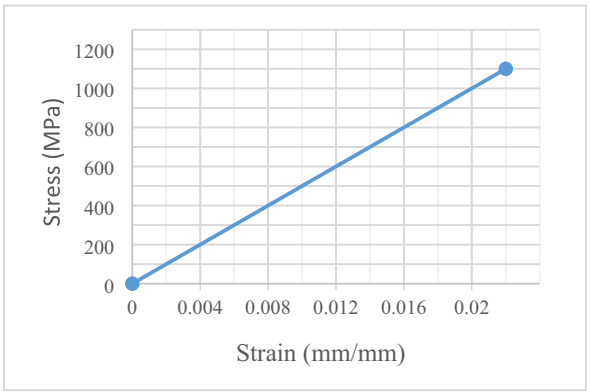

(b) GFRP bars stress-strain curve.

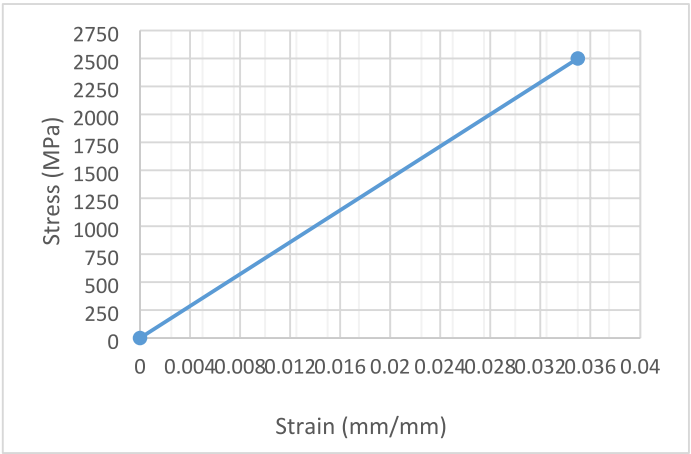

(c) GFRP sheet stress-strain curve.

Fig. 3 Concrete, GFRP bars, and GFRP sheets stress–strain curve

For example, the steel RC beam yielded 98 kN, while the GFRP RC beam attained 160 kN. The load capacity has improved by 64% when using the same amount of GFRP bar.

Wei et al. (Wei et al., 2024) studied the flexural behaviors of fiber-reinforced polymers (FRP). Wei et al. (Wei et al., 2024) concluded that the FRP bars with a greater modulus of elasticity, in addition to the increase in ρ_{sf}, increased the flexural bearing capacity of hybrid-RC beams and decreased deflection, crack width, and crack spacing of the beams. Furthermore, Wei et al. (Wei et al., 2024) concluded that the beams' ductility has greatly decreased. While reducing f_{cu} can reduces the beams' deflection and crack width, it may also improve the hybrid-RC beams' flexural bearing capacity and ductility.

Nasser et al. (Nasser et al., 2024) studied experimentally the strengthening of box-section RC beams to resist combined torsion and shear using near-surface mounts (NSM) using GFRP bars as stirrups. Nasser et al. (Nasser et al., 2024) concluded that according to the range of parameters investigated, external strengthening greatly improved the specimens' secant stiffness by 36–220%. Shear capacity is increased by 5–11% when the distance between NSM GFRP external stirrups decreases, whereas the crack load is decreased when stirrup spacing is increased.

From the previously mentioned literature review and due to the insufficiency of these studies concerning the repair and strengthening of box-section RC beams reinforced by GFRP bars using external GFRP strips, this study was done. Therefore, this study included an experimental, numerical, and analytical investigation of the behavior of RC box-section beams reinforced with GFRP bars and GFRP stirrups tested experimentally and then strengthened externally with GFRP strips. The studied parameters in this investigation are (1) the width of GFRP strips (W_f), (2) the centerline-to-centerline spacing of the strips (S_f) and (W_f/S_f) ratio, (3)

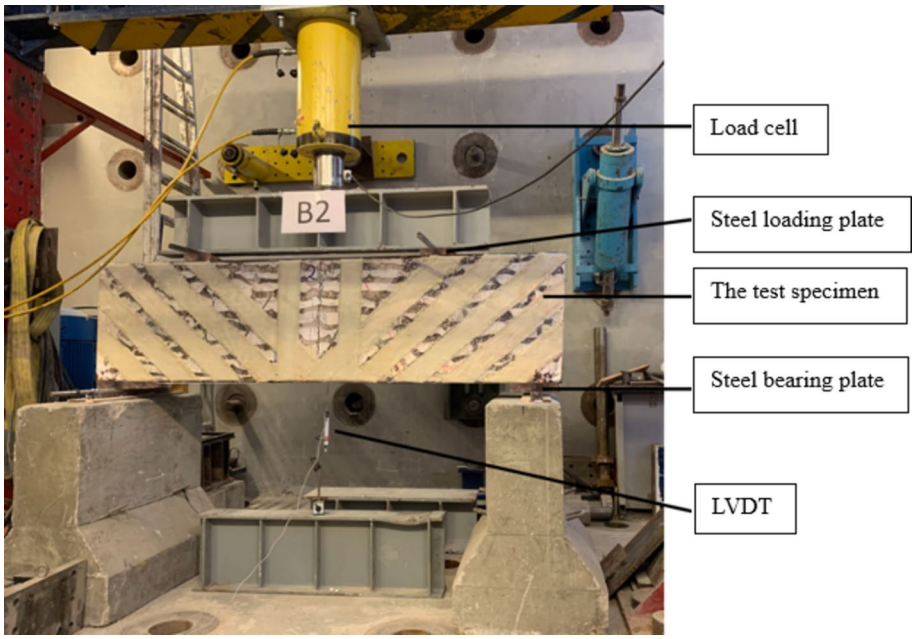

Fig. 4 Test setup and LVDT's location

Table 4 Experimental result before strengthening

Group no.	Beam symbol (before/after strengthening)	P_{cr}^{EXP} (kN)	P_{f}^{EXP} (kN)	Δ_{f}^{EXP} (mm)	Δ_{fmax}^{EXP} (mm)	Toughness (K) (kN.mm)	Secant stiffness (S.S) (kN/mm)	Displacement ductility (D.D) (mm/mm)	Failure mode
1	**B1 / $B_{1,1,150,100,45}$**	210	439.90	5.65	6.10	1401.40	77.86	1.25	D.S.F
	B2 / $B_{1,3,150,100,45}$	205	668.35	15.19	15.97	2600.03	44.00	1.32	D.S.F
	B3 / $B_{1,2,150,100,45}$	152	447.38	11.75	12.04	1012.59	38.07	1.10	D.S.F
2	**B4 / $B_{2,1,200,100,45}$**	169	557.53	13.30	14.03	1656.21	41.92	1.27	D.S.F
	B5 / $B_{2,1,100,100,45}$	179	698.27	13.63	14.28	2272.81	51.23	1.22	D.S.F
3	**B6 / $B_{3,1,150,125,45}$**	179	698.27	15.88	16.43	2415.76	43.97	1.27	D.S.F
	B7 / $B_{3,1,150,75,45}$	180	553.45	10.73	11.79	1611.61	51.58	1.26	D.S.F
4	**B8 / $B_{4,1,150,100,60}$**	190	607.84	12.92	14.05	1622.47	47.05	1.34	D.S.F
	B9 / $B_{4,1,150,100,90}$	190	584.73	11.25	11.31	1513.51	51.98	1.30	D.S.F

D.S.F. diagonal shear failure

the GFRP layers, and (4) the inclination of GFRP strips. In addition, this study investigated the most effective parameters for the behavior of the strengthened beams and compared the experimental results with those from the numerical models generated by the ANSYS program. The authors used the analytical models from the code provisions to apply a parametric study and studied the effects of some parameters on the beam's behavior.

2 Experimental Study

2.1 Test Specimens' Description

The nine tested beams have a constant total length of 2200 mm, center to center of the supporting plates

(a) Specimen $\mathbf{B_{1,1,150,100,45}}$

(b) Specimen $\mathbf{B_{1,3,150,100,45}}$

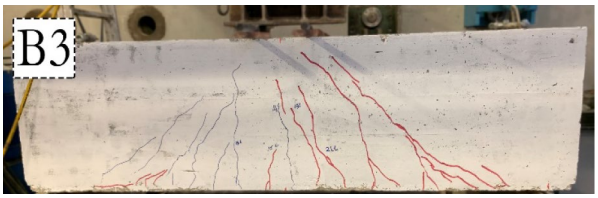

(a) Specimen $\mathbf{B_{1,2,150,100,45}}$

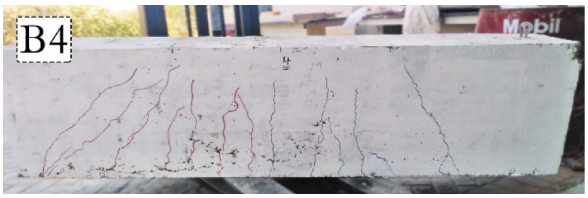

(b) Specimen $\mathbf{B_{2,1,200,100,45}}$

(e) Specimen $\mathbf{B_{2,1,100,100,45}}$

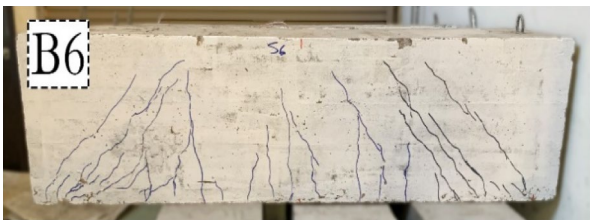

(f) Specimen $\mathbf{B_{3,1,150,125,45}}$

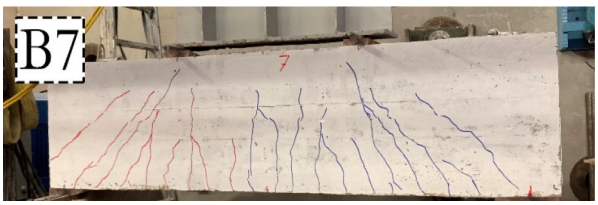

(g) Specimen $\mathbf{B_{3,1,150,75,45}}$

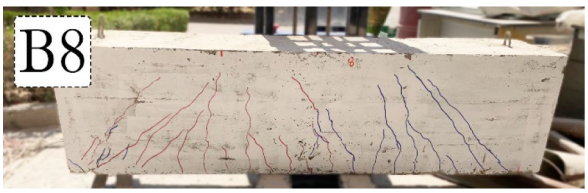

(h) Specimen $\mathbf{B_{4,1,150,100,60}}$

(I) Specimen $\mathbf{B_{4,1,150,100,90.}}$

Fig. 5 Crack patterns before strengthening

of 2000 mm, 600 mm depth, 400 mm width, and a concrete cover of 20 mm. The beams were tested as simply supported. Steel plates (200 mm * 200 mm * 25 mm) and (100 mm * 100 mm * 25 mm) were used at the bearing and loading points, as shown in Fig. 1. Solid RC sections (stiffeners) were made at the loading and bearing positions to prevent local failure. To measure the deflection at the mid-span, one linear variable differential transducer (LVDT) was used. Details of the tested beams before repair and strengthening are shown in Table 1. Table 2 and Fig. 2 show all the strengthening details. ECP 208-2019 code (ECP, 2019) was used to design the specimens. The specimens were divided into four groups. The first group contains

a) Concrete cover separation (beam $\mathbf{B_{2,1,200,100,45}}$).

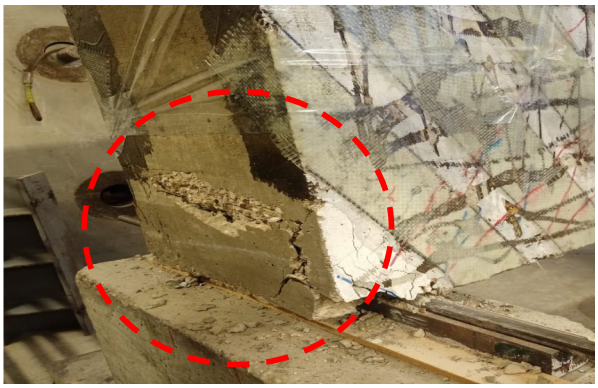

b) Failure at the support region (bearing failure mode) (beams $\mathbf{B_{1,1,150,100,45}}$, $\mathbf{B_{1,3,150,100,45}}$, $\mathbf{B_{1,2,150,100,45}}$, $\mathbf{B_{3,1,150,125,45}}$, $\mathbf{B_{4,1,150,100,90}}$, and $\mathbf{B_{3,1,150,75,45}}$).

c) Separation (debonding) of the GFRP strips (beams $\mathbf{B_{2,1,100,100,45}}$ and $\mathbf{B_{4,1,150,100,60}}$).

Fig. 6 Failure modes

Table 5 The experimental result after strengthening

Group no.	Beam symbol (before/after strengthening)	P_{cr}^{EXP} (kN)	P_f^{EXP} (kN)	Δ_f^{EXP} (mm)	Δ_{fmax}^{EXP} (mm)	Toughness (K) (kN.mm)	Secant stiffness (S.S) (kN/mm)	Displacement ductility (D.D) (mm/mm)	Failure mode
1	**B1 / $B_{1,1,150,100,45}$**	210	578.61	6.29	7.31	1137.59	92.04	1.27	End bearing
	B2 / $B_{1,3,150,100,45}$	205	820.66	23.51	24.58	3072.37	34.90	1.71	End bearing
	B3 / $B_{1,2,150,100,45}$	152	820.66	26.90	29.09	4368.71	30.51	1.55	End bearing
2	**B4 / $B_{2,1,200,100,45}$**	169	509.26	15.78	17.43	1139.51	32.28	1.48	Delamination
	B5 / $B_{2,1,100,100,45}$	179	715.27	13.44	15.13	1677.40	53.22	1.40	Debonding
3	**B6 / $B_{3,1,150,125,45}$**	179	725.47	17.45	18.01	2223.58	41.58	1.22	End bearing
	B7 / $B_{3,1,150,75,45}$	180	681.27	14.99	16.92	2146.23	45.45	1.71	End bearing
4	**B8 / $B_{4,1,150,100,60}$**	190	497.70	10.26	11.71	1182.86	48.53	1.37	Debonding
	B9 / $B_{4,1,150,100,90}$	190	762.86	19.30	20.15	2576.26	39.52	1.60	End bearing

where: K is the toughness (kN.mm), which is the ability of an element to absorb deformations up to failure, and it is equal to the area under the load–deflection curve from the initial load up to the failure load. S.S. is the secant stiffness (kN/mm.), which is the slope of the load–deflection curve and it is equal to the failure load divided by the corresponding deflection at failure. D.D. is the displacement ductility, which is the ratio of the deflection at 90% of the failure load in the descending branch to the comparable one in the ascending branch of the load–deflection curve (none dimension)

Table 6 Comparison of the experimental results before and after strengthening

Group no.	Beam symbol (before/after strengthening)	$P_{f\,after}^{EXP}/P_{f\,before}^{EXP}$ (%)	$\Delta_{f\,after}^{EXP}/\Delta_{f\,before}^{EXP}$ (%)	K/K $B_{1,1,150,100,45}$ (%)	*S.S/S.S* $B_{1,1,150,100,45}$ (%)	*D.D/D.D* $B_{1,1,150,100,45}$ (%)
1	**B1 / $B_{1,1,150,100,45}$**	132	120	100	100	100
	B2 / $B_{1,3,150,100,45}$	123	154	270	38	134
	B3 / $B_{1,2,150,100,45}$	182	242	384	33	122
2	**B4 / $B_{2,1,200,100,45}$**	91	124	100	35	116
	B5 / $B_{2,1,100,100,45}$	102	106	147	58	110
3	**B6 / $B_{3,1,150,125,45}$**	104	110	195	45	95
	B7 / $B_{3,1,150,75,45}$	124	144	189	49	134
4	**B8 / $B_{4,1,150,100,60}$**	82	83	104	53	107
	B9 / $B_{4,1,150,100,90}$	130	178	226	43	125

three specimens ($\mathbf{B_{1,1,150,100,45}}$, $B_{1,3,150,100,45}$, and $\mathbf{B_{1,2,150,100,45}}$) to study the effect of the shear span. The second group consists of two specimens ($\mathbf{B_{2,1,200,100,45}}$ and $\mathbf{B_{2,1,100,100,45}}$) to consider the effect of strip spacing (center to center of the strips). The third group contains two beams ($\mathbf{B_{3,1,150,125,45}}$ and $\mathbf{B_{3,1,150,75,45}}$) to investigate the effect of strip width. The last group consists of two beams ($\mathbf{B_{4,1,150,100,60}}$ and $\mathbf{B_{4,1,150,100,90}}$) to find the effect of strip inclination.

2.2 Material Properties and Mix Design

ASTM C39/C39M (ASTM International, 2015) was used to design the concrete mix to get a compressive strength of 30 MPa. The concrete mix, which consists of ordinary Portland cement (OPC), sand (fine aggregate), coarse aggregate (crushed stone with a maximum aggregate size of 8 mm.), and potable water, by weight, was 350, 682, 1276, and 150 kg, respectively, per one cubic meter.

ASTMC39/C39M (ASTM International, 2015) was used to find the concrete cubic compressive strength (f_{cu}) using the standard cubes (150 mm. lengths) for each specimen. ASTM C469/C496M-14 (ASTM, 2021) was used to determine the concrete cylindrical compressive strength ($f`_c$), draw the concrete stress–strain curve, and find the modules of elasticity of concrete using three standard cylinders (150 mm in diameter and 300 mm in height) for each specimen.

ASTM C496-96 (ASTM International, 2015) was used to determine the tensile strength of concrete (ft) for each specimen. The average fcu, f`c, ft, and Ec are 29.21, 23.76, 2.82, and 23,780 MPa, respectively.

The tensile mechanical properties of the used GFRP bars are shown in Table 3, according to the manufacturer's datasheet. Concrete and GFRP bars' idealized stress–strain curves are shown in Fig. 3.

2.3 Properties of GFRP Sheets and Epoxy

One, two, and three layers of unidirectional woven glass fiber sheet with a 0.3 mm/ply thickness were used, which were painted with two parts of epoxy resin on the bottom and top of the strip. The direction of the fiber sheet in the beam was vertical and inclined (90˚, 45˚, and 60˚). The properties of the GFRP sheet and epoxy resin are provided by the manufacturer. Strengthening with GFRP sheets was performed on the surface of the beams. Table 3 and Fig. 3c show the mechanical properties of the used materials.

2.4 Test Setup, Instrumentation, and Test Procedure

The beams were tested in the American University laboratory in Cairo, as shown in Fig. 4. The beams were connected to the external measuring devices, as the LVDT was installed at the mid-span of the specimen at its bottom to measure the deflection, as shown in Figs. 1 and 4. The measuring devices were calibrated before testing. Fig. 4 shows the loading setup. This system was used to record measurements at each load increment by a data acquisition system at a rate of 1 mm per minute. The specimens were loaded twice. In the first one, the beams were loaded until they reached the maximum load. After that, the beams were repaired and strengthened, and then the beams were tested for the second time, up to failure.

2.5 Strengthening Technique

The GFRP strengthening technique was used as U-wraps around the cross section of the beam with an inclination of strips to cover the shear span with two vertical strips located 100 mm from the center in all beams. The beam's surface has been roughened and cleaned to prevent brittle debonding failure or separation of concrete cover by using a roll to apply a layer of epoxy 103 with low

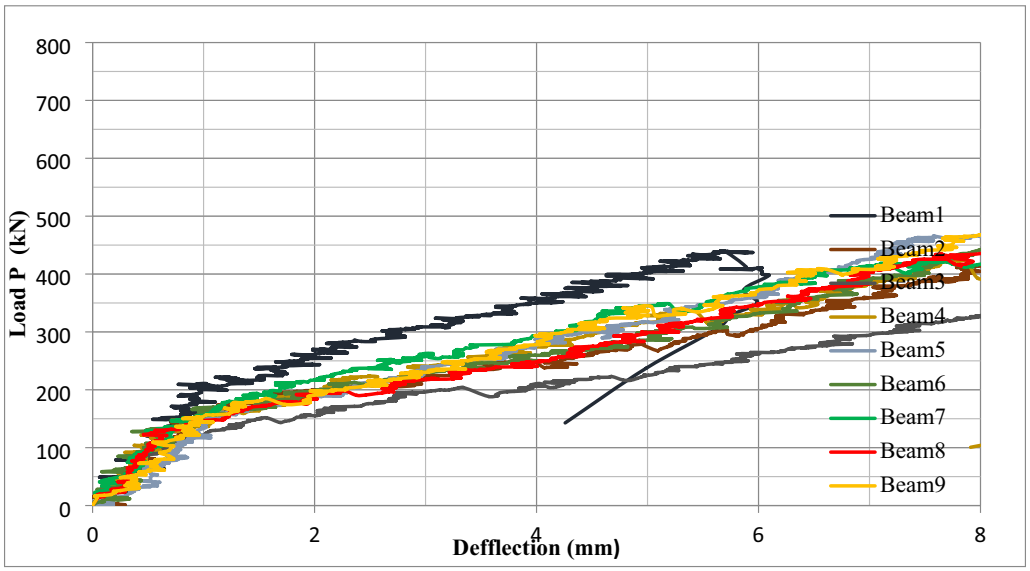

(a) Load–deflection curves for all tested beams before strengthening.

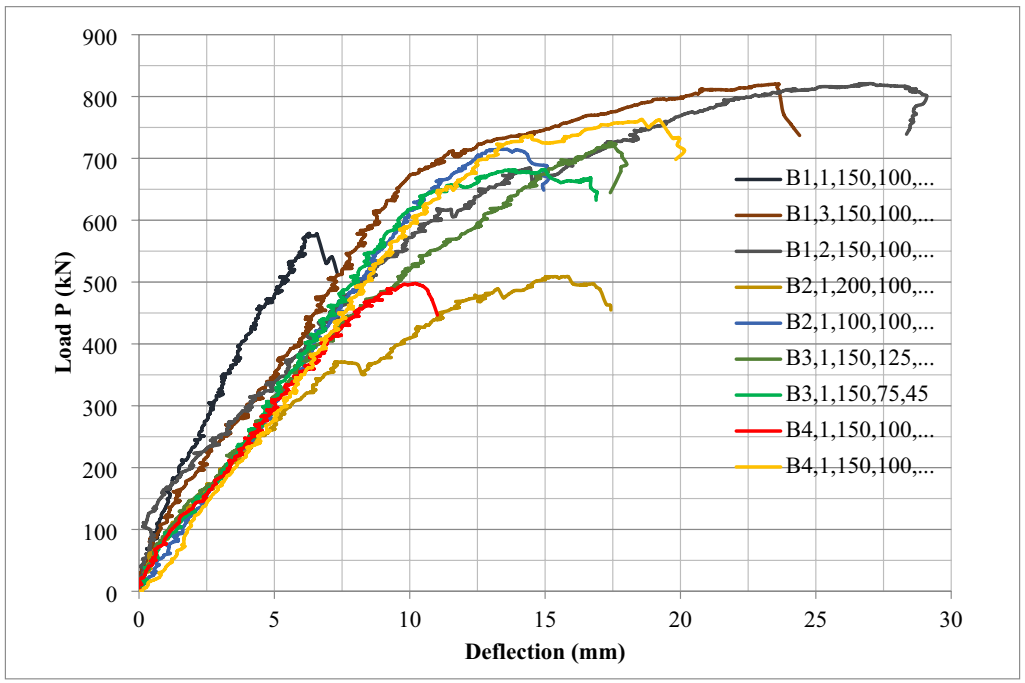

(b) Load deflection curves for all tested beams after strengthening.

Fig. 7 Load deflection curves for all tested beams before and after strengthening

density to fill the cracks and epoxy 150 and 177 to glue the strips. Two layers of epoxy were used on the strips.

3 Analysis of Results

Table 4 illustrates all the measured results, including the load at the first diagonal shear crack before strengthening (Pcr), ultimate load before and after strengthening (Pf before), (Pf after), deflection at failure load before and after strengthening (Δf), (Δf max), and percentage of

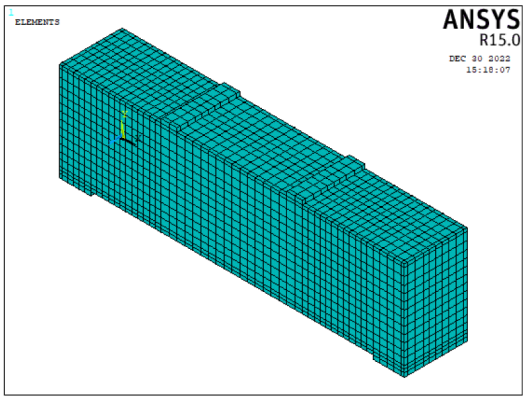

(a) Concrete, loading, and bearing plate idealizations (3-D).

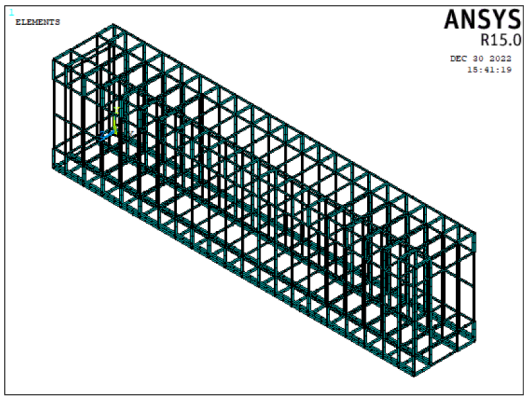

(b) Main longitudinal, secondary longitudinal reinforcement, vertical, and horizontal GFRP stirrups idealization (3-D).

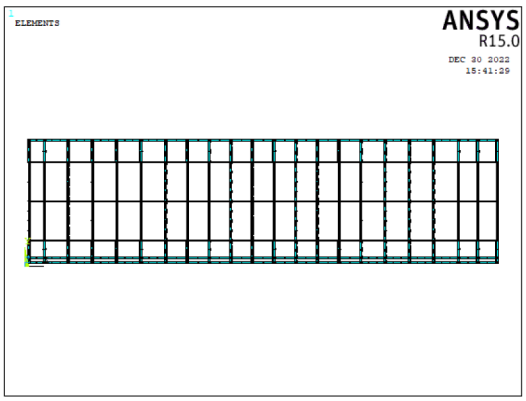

(c) Main longitudinal, secondary longitudinal GFRP reinforcement and vertical and horizontal GFRP stirrups idealization (2-D).

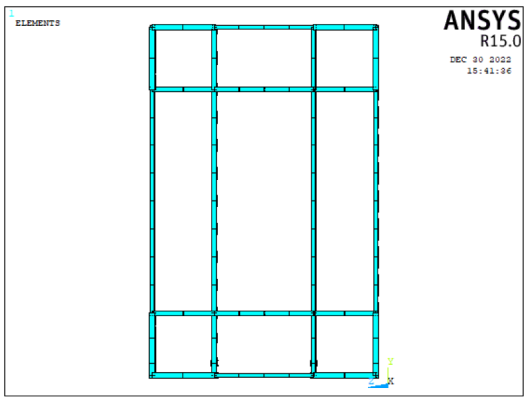

(d) Beam cross-section, vertical, and horizontal GFRP stirrups idealization (2-D).

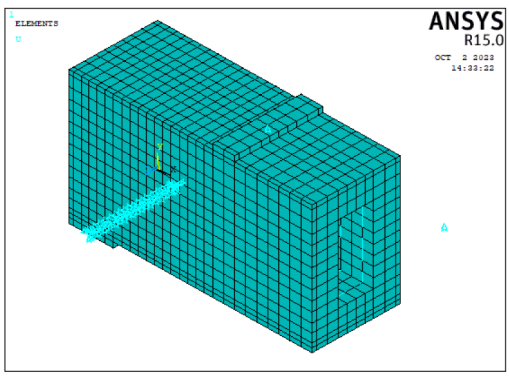

(e) Isometric of a half-beam cross-section.

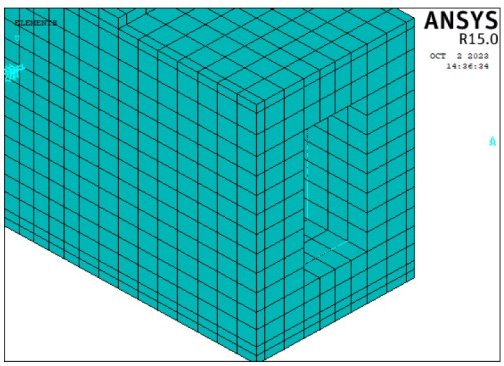

(f) A close view of the beam cross-section

Fig. 8 Idealization for tested beams by ANSYS (ANSYS, 2015)

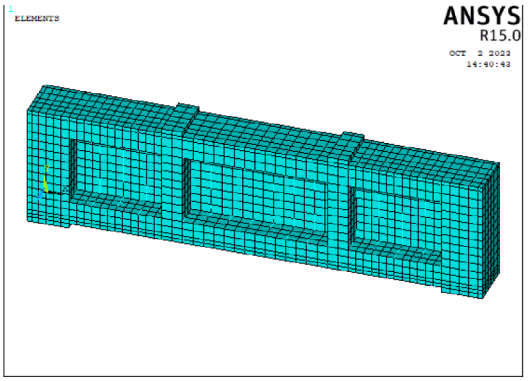

(g) Isometric of the half-beam longitudinal section.

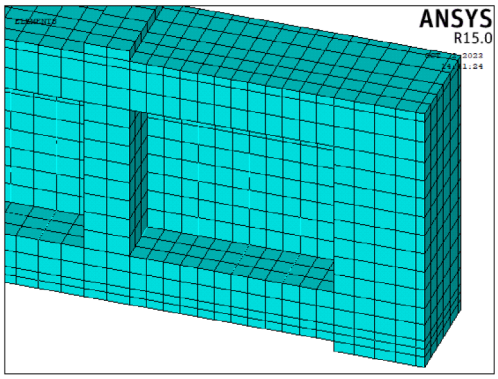

(h) A close view of the longitudinal section of the beam.

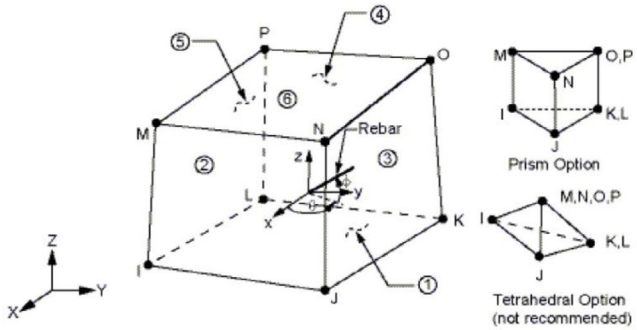

(I) Orientation angle Φ and θ.

Fig. 8 continued

the ratio Pf after/Pf before. For beams B1,1,150,100,45, B1,2,150,100,45, and B1,3,150,100,45 in group 1, when using 1, 2, and 3 layers of GFRP, respectively, the ultimate load increased by 31%, 82%, and 22%, respectively. Therefore, up to a certain limit, if the number of layers increased, the maximum load increased. This can be attributed to the separation that occurs between the layers and the concrete surface before the beam reaches the maximum load, and the effect of increasing the number of layers becomes insignificant. For beams in group 2, when increasing the spacing between strips in beams B2,1,200,100,45, the failure load decreased by 9%. When decreasing the spacing between strips in beam B2,1,100,100,45, the load was increased by 3%. For beams B3,1,150,125,45 and B3,1,150,75,45 in group 3 with strip widths of 125 mm and 75 mm, the load increased by 3.9% and 24%, respectively. This means that beam B3,1,150,125,45 is reinforced by the maximum vertical web reinforcement; therefore, the effect of strip width on the maximum load is less. In group 4, when the strip's inclination is 60̊ in beam B4,1,150,100,60, the failure load decreases by 19% due to the debonding of some strips. When the strip inclination is 90̊, in beam B4,1,150,100,90, the load increases by 30%.

3.1 Crack Patterns and the First Crack

Shear cracks began to appear near the loading point up to the supports, and the cracks appeared vertical at the mid-span. The width of diagonal shear cracks became wider with increasing load up to failure. Fig. 5 shows the crack patterns for all the tested beams.

3.2 Failure Modes

When strengthening a beam with GFRP sheets, it's crucial to consider the failure modes that can occur during the repair process. Proper installation techniques, such as applying the GFRP sheets in the correct orientation and ensuring adequate overlap, are critical for ensuring a successful repair. To prevent the failure modes, it is important to properly prepare the beam surface by cleaning, roughening, and applying a suitable

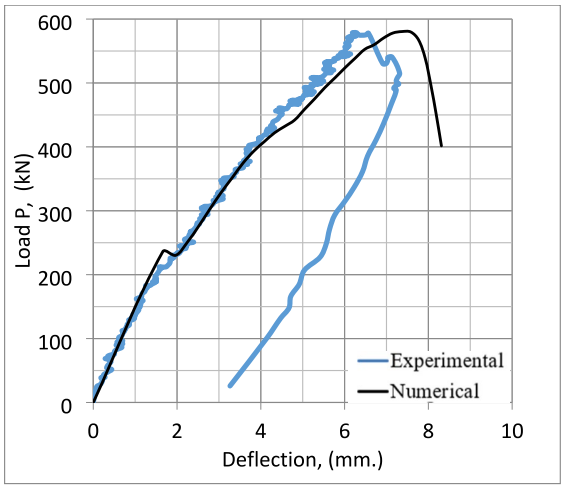

(a) Beam $\mathbf{B_{1,1,150,100,45}}$

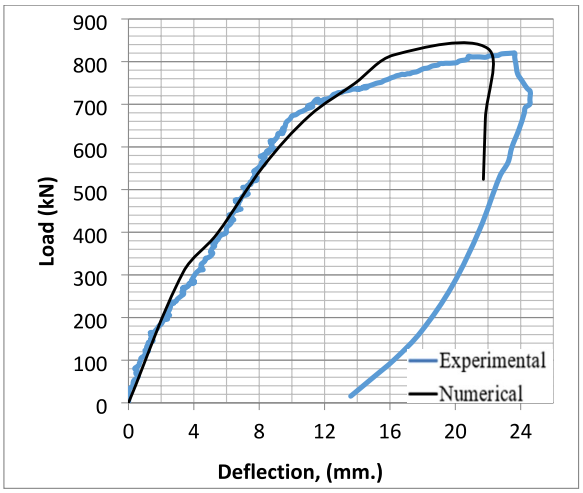

(b) Beam $\mathbf{B_{1,3,150,100,45}}$

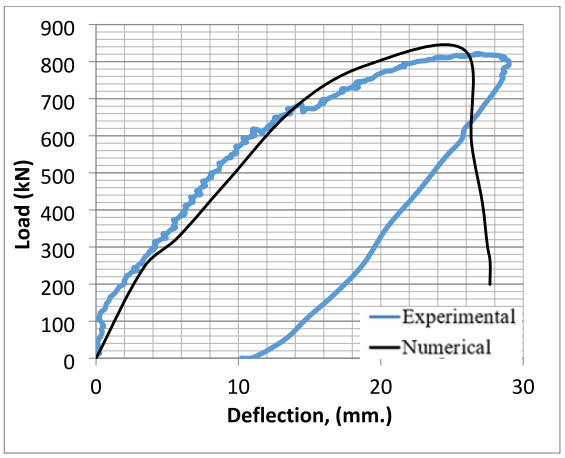

(c) Beam $\mathbf{B_{1,2,150,100,45}}$

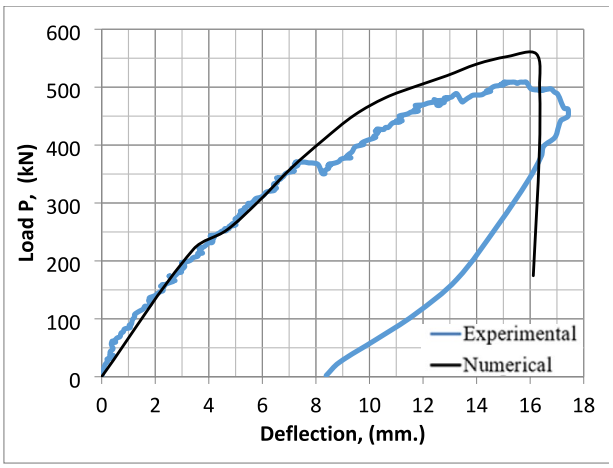

(d) Beam $\mathbf{B_{2,1,200,100,45}}$.

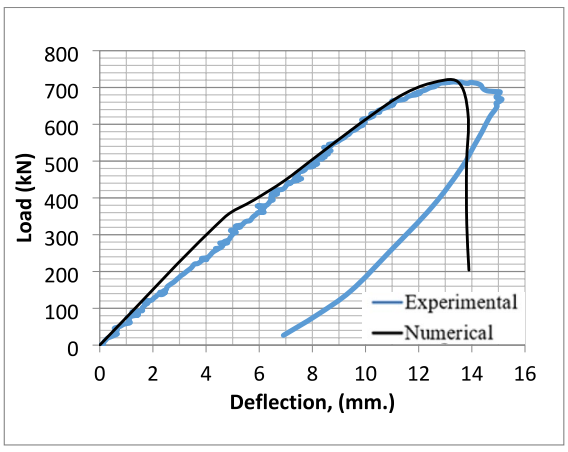

(e) Beam $\mathbf{B_{2,1,100,100,45}}$

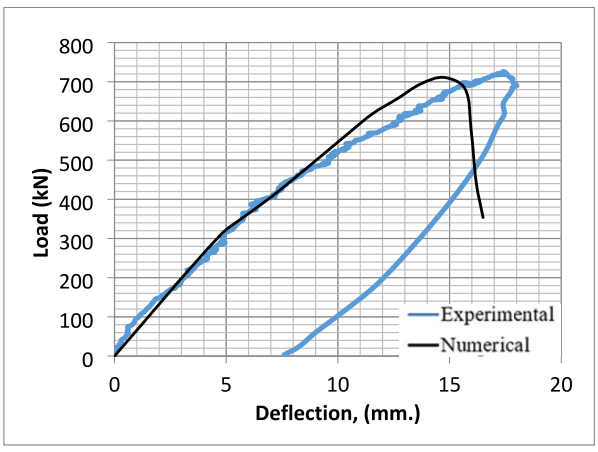

(d) (f) Beam $\mathbf{B_{3,1,150,125,45}}$

Fig. 9 Experimental and numerical load–deflection curves of all tested beams after strengthening

Table 7 Comparison between experimental and numerical results

Group no.	Beam symbol (before/after strengthening)	P_f			Deflection at failure load Δ_f		
		ANSYS (kN)	Experimental (kN)	ANSYS/Exp. %	ANSYS (mm.)	Experimental (mm.)	ANSYS/Exp. %
1	**B1 / $B_{1,1,150,100,45}$**	580.46	578.61	100.3	7.37	6.29	117
	B2 / $B_{1,3,150,100,45}$	830.83	820.66	101.2	21.99	23.51	94
	B3 / $B_{1,2,150,100,45}$	832.41	820.66	101.4	25.84	26.90	97
2	**B4 / $B_{2,1,200,100,45}$**	557.64	509.26	109.5	16.23	15.78	103
	B5 / $B_{2,1,100,100,45}$	715.93	715.27	100.0	13.47	13.44	100
3	**B6 / $B_{3,1,150,125,45}$**	711.01	725.47	98.0	14.75	17.45	85
	B7 / $B_{3,1,150,75,45}$	684.43	681.27	100.5	14.23	14.99	95
4	**B8 / $B_{4,1,150,100,60}$**	503.46	497.70	101.2	8.99	10.26	88
	B9 / $B_{4,1,150,100,90}$	782.77	762.86	102.6	18.57	19.30	96
Average				101.6			97
Standard deviation				3.0			9

where P_f and Δ_f are the ultimate load and the deflection at the ultimate load

adhesive. A concrete cover separation failure mode occurred in beam $\mathbf{B_{2,1,200,100,45}}$. Another failure mode is the bearing failure mode, which occurred for beams $\mathbf{B_{1,1,150,100,45}}$, $B_{1,2,150,100,45}$, $\mathbf{B_{1,3,150,100,45}}$, $\mathbf{B_{3,1,150,125,45}}$, $\mathbf{B_{4,1,150,100,90}}$, and $B_{3,1,150,75,45}$. The collapse occurred in the GFRP strips when increasing applied loads then a failure in concrete at the support region occurred. One of the potential failure modes is debonding failure mode, which is the separation of the GFRP sheets from the beam's surface due to inadequate bonding (separation of the GFRP strips) such as the failure mode occurred to beams $\mathbf{B_{2,1,100,100,45}}$ and $\mathbf{B_{4,1,150,100,60}}$. The delamination failure mode, which occurs when the layers of the GFRP sheets separate from each other did not occur for beams $\mathbf{B_{1,2,150,100,45}}$ and $\mathbf{B_{1,3,150,100,45}}$ have two and three layers. Fig. 6 shows the observed failure modes.

3.3 Ultimate Loads and Load–Deflection Curves

The experimental failure loads and load–mid-span deflection curves before and after strengthening are shown in Fig. 7. The curves are bilinear. The curves consist of two parts. The first part shows the behavior before cracking, and the second part represents the behavior after cracking occurs. The deflection at failure load is shown in Table 5. The percentage of maximum deflection after strengthening/maximum deflection before strengthening for beams B1,1,150,100,45, B1,2,150,100,45, and B1,3,150,100,45 when using 1, 2, and 3 layers of GFRP, respectively, increased by 20%, 54%, and 142%. In group 2, by increasing the spacing between strips in beam B2,1,200,100,45, the percentage of maximum deflection increased by 24%, and when decreasing the spacing between strips in beam B2,1,100,100,45, the percentage of maximum deflection increased by 6%, which means more warnings before failure. For beams B3,1,150,125,45 and B3,1,150,75,45, when using strips with widths of 125 and 75 mm, the percentage of maximum deflection increased by 10% and 44%, respectively. In group 4, when the strip inclination is 60̊ in beam B4,1,150,100,60, the percentage of maximum deflection decreased by 17% due to the debonding failure, and when the strip inclination is 90̊ in beam B4,1,150,100,90, the percentage of maximum deflection increased by 78%; therefore, the failure takes time to occur, as shown in Table 6.

3.4 Secant Stiffness, Toughness, and Displacement Ductility

Table 5 shows all the measured experimental results, including toughness (K), secant stiffness (S.S.), displacement ductility (D.D.), and failure load (Pf). For beams in group 1, when using two and three layers of GFRP, the displacement ductility increased by 22% and 34%, respectively, compared to the control specimen with one layer. For beams in group 2, when increasing the spacing between strips by 100%, the toughness decreased by 47%, the secant stiffness decreased by 23%, and the displacement ductility increased by 7%. For beams in group 3, when increasing the width of the strips by 40%, the toughness increased by 7%, the secant stiffness decreased by 5%, and the displacement ductility decreased by 39%.

4 Numerical Analysis

To simulate the repair and strengthening of box-section RC beams reinforced by GFRP bars using GFRP strips. A nonlinear finite element analysis was conducted using the ANSYS program (ANSYS, 2015). The studied

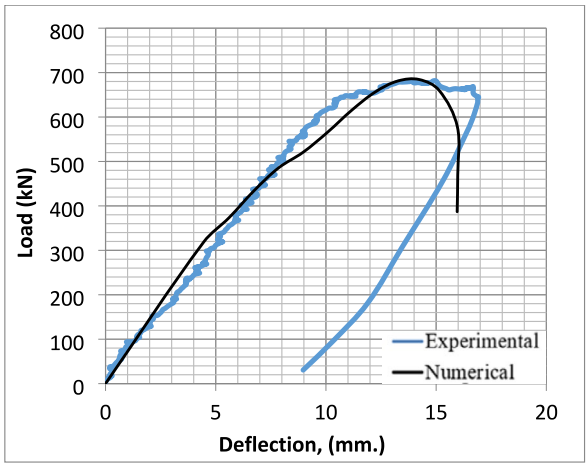

(g) Beam $\mathbf{B_{3,1,150,75,45}}$

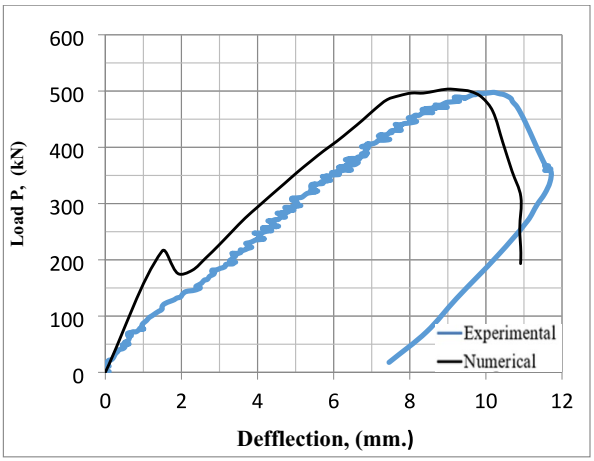

(h) Beam $\mathbf{B_{4,1,150,100,60}}$

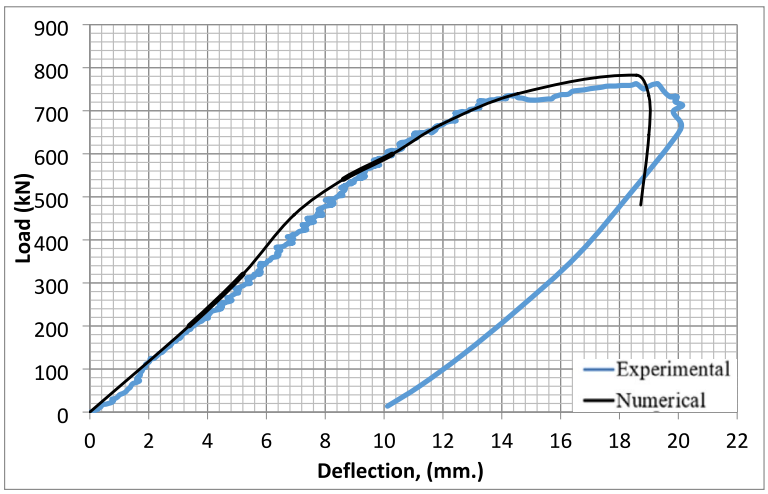

(i) Beam $\mathbf{B_{4,1,150,100,90}}$

Fig. 9 continued

variables are (1) the number of layers (N) (1, 2, and 3), (2) the spacing between strips (S) center to center (100 and 200 mm), (3) the strip width (125 and 75 mm.), and (4) the inclination of strips (θ) (450, 600, and 900 degrees). Because the load–deflection curve indicates various response parameters, including ultimate load, deflection, cracks, etc., it is considered to be the most important variable in studying the behavior of RC beams.

4.1 Elements, Loads, Material Models, and Boundary Conditions

An eight-node element (SOLID65) with three translational degrees of freedom at each node is used for modeling concrete. SOLID65 element characteristics, including cracking, were considered. The specimens were modeled using a cubic mesh with a size of 25 mm. To model GFRP bars and GFRP stirrups, the Link180 element, which has three transition degrees of freedom at each node, was used. The bond between concrete and the GFRP bars and GFRP sheets was assumed to be perfect. Steel plates were modeled using SOLID185 for loading and bearing plates. To simulate the strips, the real constants were used to identify the volumetric ratio and orientation angles Φ and θ for all volumes, as shown in Fig. 8.

Concrete in tension is represented using a bilinear-softening (trilinear) model, and concrete in compression is illustrated by the unconfined concrete model. The GFRP bars, GFRP stirrups, and GFRP sheets were idealized by linear modeling (ANSYS, 2015), as shown in Fig. 3. The

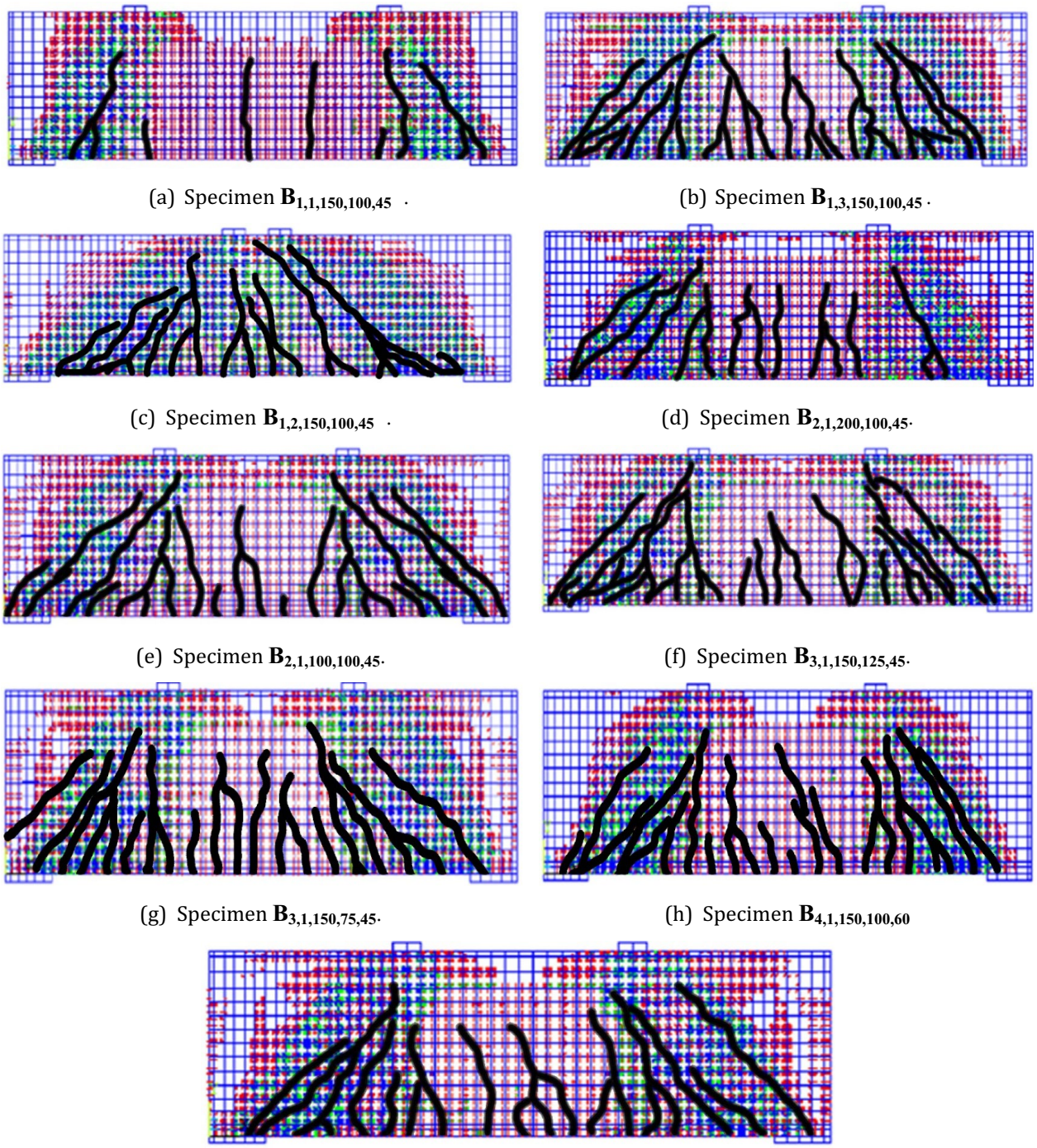

(a) Specimen $\mathbf{B_{1,1,150,100,45}}$.

(b) Specimen $\mathbf{B_{1,3,150,100,45}}$.

(c) Specimen $\mathbf{B_{1,2,150,100,45}}$.

(d) Specimen $\mathbf{B_{2,1,200,100,45}}$.

(e) Specimen $\mathbf{B_{2,1,100,100,45}}$.

(f) Specimen $\mathbf{B_{3,1,150,125,45}}$.

(g) Specimen $\mathbf{B_{3,1,150,75,45}}$.

(h) Specimen $\mathbf{B_{4,1,150,100,60}}$

(I) Specimen $\mathbf{B_{4,1,150,100,90}}$.

Fig. 10 Predicted failure modes and crack patterns of all tested specimens after strengthening

Table 8 Comparison of experimental, numerical, and analytical results after strengthening

Beam No.	Results														
	P_u^{ECP} (kN)	P_u^{ACI}(kN)	P_u^{EUR}(kN)	P_u^{Num} (*kN*)	P_f^{EXP}(kN)	$\frac{P_u^{ECP}}{P_f^{EXP}}$	$\frac{P_u^{ACI}}{P_f^{EXP}}$	$\frac{P_u^{EUR}}{P_f^{EXP}}$	$\frac{P_u^{Num}}{P_f^{Exp}}$	$\frac{P_u^{ECP}}{P_u^{Num}}$	$\frac{P_u^{ACI}}{P_u^{Num}}$	$\frac{P_u^{EUR}}{P_u^{Num}}$	$\frac{P_u^{ECP}}{P_u^{ACI}}$	$\frac{P_u^{ECP}}{P_u^{EUR}}$
$B_{1,1,150,100,45}$	689	596	568	580	579	1.19	1.03	0.98	1.00	1.19	1.03	0.98	1.16	1.21
$B_{1,3,150,100,45}$	808	833	806	831	821	0.98	1.02	0.98	1.01	0.97	1.00	0.97	0.97	1.00
$B_{1,2,150,100,45}$	717	653	701	832	821	0.87	0.80	0.85	1.01	0.86	0.78	0.84	1.10	1.02
$B_{2,1,200,100,45}$	669	545	590	558	509	1.31	1.07	1.16	1.10	1.20	0.98	1.06	1.23	1.13
$B_{2,1,100,100,45}$	729	686	535	716	715	1.02	0.96	0.75	1.00	1.02	0.96	0.75	1.06	1.36
$B_{3,1,150,125,45}$	1245	1028	690	711	725	1.72	1.42	0.95	0.98	1.75	1.45	0.97	1.21	1.80
$B_{3,1,150,75,45}$	910	693	673	684	681	1.34	1.02	0.99	1.00	1.33	1.01	0.98	1.31	1.35
$B_{4,1,150,100,60}$	707	591	589	503	498	1.42	1.19	1.18	1.01	1.40	1.17	1.17	1.20	1.20
$B_{4,1,150,100,90}$	722	549	520	783	763	0.95	0.72	0.68	1.03	0.92	0.70	0.66	1.31	1.39
Mean						1.14	0.97	0.94	1.02	1.11	0.95	0.93	1.17	1.28
Standard Deviation						0.19	0.14	0.16	0.03	0.18	0.14	0.15	0.11	0.23

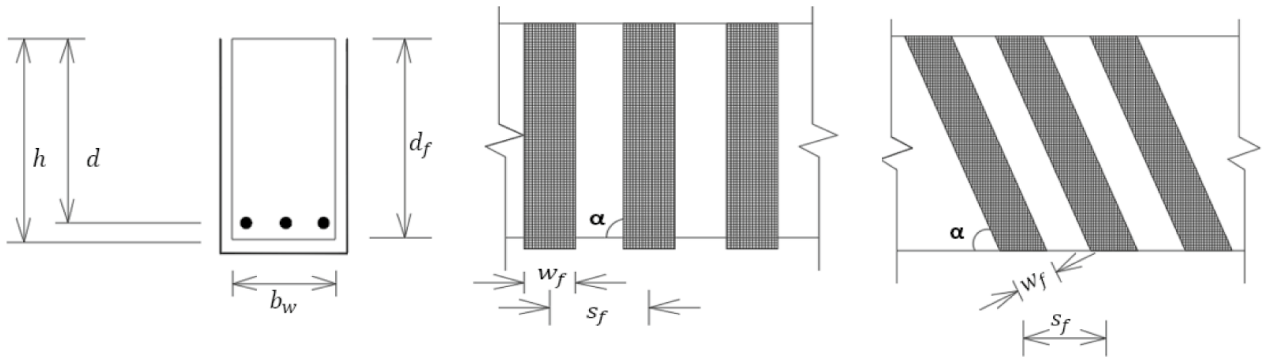

(a) Cross-section. (b) α = 90°. (c) α < 90°.

Fig. 11 Definition of the variables when calculating the shear strength using GFRP strips

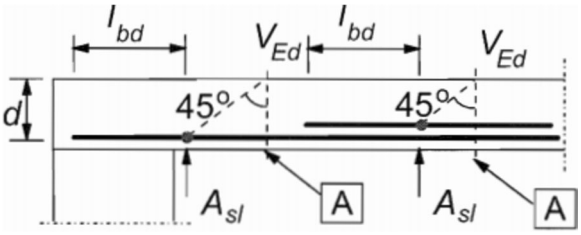

Fig. 12 Definition of Asl

studied specimens were modeled as simply supported beams under four-point loading with hinged support at one side and roller support at the other side of the beam.

4.2 Validation Model

The numerical results shown in Fig. 9 have been verified by comparing the experimental and numerical results. Table 7 compares the deflections at failure and ultimate loads of the tested beams for experimental and numerical results. The measured and predicted load–deflection curves show good agreement, as shown by the mean and standard deviation. The average percentage of the numerical ultimate loads to the experimental failure loads is 102%, and the standard deviation percentage is 3%. These values are 97% and 9% for deflections at failure loads. The results show satisfactory agreement between numerical and experimental output. Figs. 5 and 10 show an agreement between the numerical and observed crack patterns from the experimental results.

4.3 Parametric Study

The effect of the number of layers was studied. When using two layers of GFRP is the optimum solution to avoid the debonding and delamination of GFRP layers. The number of layers increases the maximum load, but when the layers increase up to a certain limit, separation occurs between the layers and the concrete surface before the beam reaches the maximum load, and the effect of increasing the number of layers becomes less. The effect of strip spacing was investigated and the results showed that when decreasing the spacing between strips, the load was increased. In addition, the effect of the width of strips was studied, where the results showed that the load-carrying capacity increased with the increase of the strip's width. The effect of strip inclination was also investigated, and the results showed that when the strip inclination is 60̊ in beam $B_{4,1,150,100,60}$, the ultimate load decreases by 19% due to the debonding of some strips, and when the strip inclination is 90̊, in beam $B_{4,1,150,100,90}$, the load increases by 30%.

5 Comparison with Guidelines

5.1 Comparison with Egyptian Code ECP 208–19 (ECP, 2019)

The ultimate shear strength of the GFRP strips is given in Eq. (1):

$$q_{fu} = \frac{A_f * E_f * \varepsilon_{ef} * (sin\alpha) * \left(\frac{d_f}{d}\right)}{S_f * b_w} \leq 4N/mm^2 \quad (1)$$

$$A_f = 2n * t_f * w_f \quad (2)$$

$$\varepsilon_{ef} = 0.004 \leq .75\varepsilon_{fu} \quad (3)$$

where:

A_f: the area of the strips.
E_f: the modulus of elasticity of the strips.
ε_{ef}: the effective strain of the strips.
ε_{fu} : the ultimate strain of the strips.
α: the inclination angle of the strips.
d: the beam's depth.
df: the depth of the strips.
Ss: the distance between the centers of the strips.
b_w : the beam width.
n: the number of layers.
t_f: the thickness of the strips.
w_f : the width of the strips.

The comparison between the experimental failure load and the predicted ultimate load calculated according to the ECP 208–19 code (ECP, 2019) is shown in Table 8. The mean of the ratio of the ECP 208–19 (ECP, 2019) ultimate loads and the numerical predicted loads to the experimental failure loads is 1.14 and 1.11, respectively, while the standard deviations are 0.19 and 0.18, respectively.

5.2 Comparison with the American Code ACI 440-2R-17 (2017)

The GFRP contribution in shear is given by the following equation:

$$v_f = \frac{A_{fv} * F_{fe} * (sin\alpha + cos\alpha) * d_{fv}}{S_f} \quad (4)$$

where α is the inclination angle of the GFRP strips, S_f is the spacing of the centers of the strips, d_{fv} is the depth of the GFRP strips, and A_{fv} is the total GFRP area as shown in Fig. 11, which is given by

$$A_{fv} = 2n * t_f * w_f \quad (5)$$

where n is the number of the GFRP layers, t_f is the thickness of the strips, and w_f is the width of the strips.

The tensile stress in the strips (nominal strength) is given by the following equation:

$$F_{fe} = E_f * \varepsilon_{fe} \quad (6)$$

E_f is strip's modulus of elasticity and ε_{fe} is the strain in the strips.

The maximum strain in the strips is given by the following equation:

$$\varepsilon_{fe} = 0.004 \leq .75\varepsilon_{fu} \quad (7)$$

For the U-wrapped shape, the strain is given by the following equation:

$$\varepsilon_{fe} = k_v * \varepsilon_{fu} \leq 0.004 \quad (8)$$

where k_v is the strain reduction coefficient, which is given by Eq. (9):

$$k_v = \frac{k_1 * k_2 * l_e}{11900 * \varepsilon_{fu}} \leq .75 \quad (9)$$

$$l_e = \frac{23300}{(n * t_f * E_f)^{0.58}} \quad (10)$$

where l_e is the bond length:

$$k_1 = \left(\frac{f_{c\prime}}{27}\right)^{\frac{2}{3}} \quad (11)$$

$$k_2 = \frac{d_{fv} - l_e}{d_{fv}} \text{ for U wraps} \quad (12)$$

5.3 Comparison with the Eurocode (B. S. & Eurocode, 2004)

The design value for the shear resistance V $_{Rd,c}$ for unreinforced sections is given by

$$V_{Rd,c} = \left[C_{Rd,c} k (100 \rho_1 f_{ck})^{1/3} + k_1 \sigma_{cp}\right] b_w.d \quad (13)$$

$$C_{Rd,c} = 0.18/\gamma_c \quad (14)$$

Assuming

$$\sigma_{cp} = 0.0 \quad (15)$$

$$k = 1 + \sqrt{\frac{200}{d}} \leq 2.0 \quad (16)$$

Assuming 50% of the mid-span reinforcement extended up to the supports, as shown in Fig. 12:

$$\rho 1 = \frac{Asl}{bwd} \leq 0.02 \quad (17)$$

where:

$V_{Rd,c}$: is the design value for the shear resistance without shear reinforcement.

A_{SL}: is the area of the tensile reinforcement, which extends $\geq (I_{bd} + d)$ beyond the considered section, as shown in Fig. 12.

l_{bd}: is the anchorage length according to B. S. and Eurocode (2004).

b_w: is the smallest width of the cross section in the tensile area (mm.).

d: is the beam's effective depth in mm.

f_{ck}: is the compressive strength of concrete in MPa.

k_1: is a factor that depends on the depth.

σ_{cp}: is the concrete compressive stress at the centroidal axis due to axial loading.

$\gamma_{c:}$ is the strength reduction factor for concrete.

$$V_{Rd,s} = \frac{A_{sw}}{S} Z f_{ywd} \cot \theta \quad (18)$$

$V_{Rd,s}$: is the shear resistance for members with vertical shear reinforcement.

A_{sw}: is the cross-sectional area of the shear reinforcement.

S: is the spacing of the stirrups.

f_{ywd}: is the design yield strength of the shear reinforcement.

Θ: is the angle between the concrete compression strut and the beam axis perpendicular to the shear force.

Z: is the inner lever arm for a member with constant depth in the shear analysis of reinforced concrete. The approximate value Z = *0.9d* may normally be used.

$$V_{Rd,f} = [0.9 \varepsilon_{fk,e} / \Upsilon_f E_f \rho_f b_{w.} d. (1 + \cot \beta) \sin \beta \quad (19)$$

$$e_{fke} = 65 (\frac{f_c^{\frac{2}{3}}}{E_f \rho_f}) 0.56 \quad (20)$$

$V_{Rd,f}$: is the shear contribution of FRP.

β: is the angle of inclination of FRP fibers to the longitudinal axis of the member.

$\varepsilon_{fk,e:}$ is the effective tensile strain of FRP.

Υ_f: is the partial safety factor for FRP.

E_f: is the modulus of elasticity of the FRP.

ρ_f: is the FRP reinforcement ratio.

f_c: is the compressive strength of concrete in MPa.

6 Analysis of the Results

Table 8 shows the predicted ultimate load P_u according to the Egyptian code ECP 208–19 (ECP, 2019), the American code ACI 440-2R-17 2017, and Eurocode (B. S. & Eurocode, 2004) compared to experimental and numerical ones.

When comparing the results from the three code provisions [18, 23, and 24] and the numerical results from the ANSYS program to the experiment results of the tested specimens, the average of the ratios of $\frac{P_u^{ECP}}{P_f^{EXP}}, \frac{P_u^{ACI}}{P_f^{EXP}}, \frac{P_u^{EUR}}{P_f^{EXP}}$, and $\frac{P_u^{Num}}{P_f^{Exp}}$ are 1.14, 0.97, 0.94, and 1.02, respectively, and the standard deviations for the same ratios are 0.19, 0.14, 0.16, and 0.03, respectively. That means that the American code ACI 440–19 (2017) and Eurocode (B. S. & Eurocode, 2004) are more conservative than the Egyptian code ECP 208–19 (ECP, 2019), and the numerical analysis gives good results. The ACI code and Eurocode shear equations do not consider variations in the shear span or the dowel action of the main, secondary, and side horizontal reinforcement, so this is the reason for their higher standard deviations. The Egyptian code ECP 208–19 (ECP, 2019), ACI 4401R15 (2017), and Eurocode (B. S. & Eurocode, 2004) considered the effect of main reinforcement by using the k-factor, which is the ratio of the depth of the neutral axis (N.A.), in the shear equation.

By comparing the results from the three code provisions [ECP, 2019; ACI 4401R15 2017; B. S. & Eurocode, 2004 to the numerical results from the ANSYS program for the tested specimens, the average of the ratios . $\frac{P_u^{ECP}}{P_u^{Num}}, \frac{P_u^{ACI}}{P_u^{Num}}$, and $\frac{P_u^{EUR}}{P_u^{Num}}$ are 1.11, 0.95, and 0.93, respectively, and the standard deviations for the same ratios are

0.18, 0.14, and 0.15, respectively, which confirms the previous conclusion.

The comparison of results from the three code provisions [18, 23, and 24] through the average ratios and standard deviations of the ratios $\frac{P_u^{ECP}}{P_u^{ACI}}$ and $\frac{P_u^{ECP}}{P_u^{EUR}}$ show that the Egyptian code ECP 208–19 (ECP, 2019) is unconservative compared to the ACI 4401R15 2017, and Eurocode (B. S. & Eurocode, 2004) codes.

7 Conclusions

From the experimental, numerical, and analytical results for the ranges of the studied parameters, the following conclusions can be drawn:

1. Compared with the beam before strengthening when using one, two, and three layers of GFRP, the failure load increased by 31%, 82%, and 22%, respectively. Therefore, using two layers of GFRP is the optimum solution to avoid the debonding and delamination of GFRP layers.
2. The number of layers increases the failure load, but when the layers increase to more than two layers, separation occurs between the layers and the concrete surface before the beam reaches the failure load, and the effect of increasing the number of layers becomes insignificant.
3. Increasing the spacing between strips decreased the failure load by 9% and the mode of failure that occurred was delamination and the beam failed in flexural shear.
4. When increasing the spacing between strips, the percentage of maximum deflection increased by 6%, which gives more warnings before failure.
5. Increasing the width of strips increases the load-carrying capacity by 6% for the studied values.
6. Compared with the beam after strengthening to that before strengthening, when the strip inclination is 90, the failure load increased by 18%. When the strip inclination is 60, the failure load increases by 30% and the effect of strips with angle 60 was better than that with angle 90 in improving the load.
7. The crack patterns and load–deflection curves show consistency between the experimental results and those from the numerical results using ANSYS models.
8. The experimental results and the nonlinear finite element results using the ANSYS program showed a good agreement, where the average value of the failure load from $\frac{\text{ANSYS}}{\text{Exp}}$% and the displacement at failure from $\frac{\text{ANSYS}}{\text{Exp}}$% are 102% and 97%, respectively, and a standard deviation of 3% and 9%.
9. By comparing the results from the three code provisions (the ACI 440–19 code, the Egyptian code ECP 208–19, and Eurocode) and the numerical results from the ANSYS program to the experiment results of the tested specimens, the average of the ratios of $\frac{P_u^{ECP}}{P_f^{EXP}}$, $\frac{P_u^{ACI}}{P_f^{EXP}}$, $\frac{P_u^{EUR}}{P_f^{EXP}}$, and $\frac{P_u^{Num}}{P_f^{Exp}}$ are 1.14, 0.97, 0.94, and 1.02, respectively, and the standard deviations for the same ratios are 0.19, 0.14, 0.16, and 0.03, respectively. This means that the American code ACI 440–19 and Eurocode are more conservative than the Egyptian code ECP 208–19, and the numerical analysis gives good results.
10. The comparison of results from the three code provisions (the ACI 440–19 code, the Egyptian code ECP 208–19, and Eurocode) through the average ratios and standard deviations of the ratios $\frac{P_u^{ECP}}{P_u^{ACI}}$ and $\frac{P_u^{ECP}}{P_u^{EUR}}$ show that the Egyptian code ECP 208–19 is unconservative compared to the ACI 4401R15, and Eurocode codes.

8 Recommendations for Future and Further Investigations

1. An extensive experimental investigation is required to determine how various types of FRP strips affect the behavior and strengthening of box-section RC beams reinforced by GFRP bars.
2. Conduct a cost analysis to find the cheapest and best type of FRP strips.
3. Apply other methods of external strengthening such as using an FRP rope immersed in the epoxy raisin and implemented as a near-surface-mount (NSM) around the beam section, equivalent to external stirrups with different diameters, spacings, inclinations, and strengths.

8.1 Research Significant

– Studying experimentally, numerically, and analytically the behavior of RC box-section beams reinforced with GFRP bars and GFRP stirrups and strengthened externally with GFRP strips;

- Investigating the most effective parameters for the behavior of the strengthened beams.
- Comparing the experimental results with those from the numerical models generated by the ANSYS program; and
- -Using the analytical models from the code provisions to perform a parametric study, comparing its results with the experiment and numerical results, and studying the effects of some parameters on the studied beam's behavior.

Acknowledgements
The authors carried out the experimental work in the laboratory of the American University laboratory in Cairo, Egypt. The authors acknowledged the help and assistance offered by the laboratory staff.

Author contributions
All the authors declare their contributions to the paper preparation (experimental/numerical activities, discussions, and paper reading and writing). Ahmed A. Mahmoud, corresponding author Actively participated in the research plan and assisted in how to implement the practical and theoretical program and review the paper. Conceptualization, methodology, project administration, validation, supervision, writing, reviewing, and editing the paper. Manar S. Sedeek Implemented the experimental and analytical programs. Data curation includes formal analysis, funding acquisition, investigation, and writing the original draft. Mohamed A. Salama Carried out a technical and linguistic review of the paper before submitting it, methodology, software, supervision, and writing the original draft. Ahmed N. M. Khater Check the paper carefully, review it, and try to make it in the final form. Resources, software supervision, and writing the original draft.

Funding
Open access funding provided by The Science, Technology & Innovation Funding Authority (STDF) in cooperation with The Egyptian Knowledge Bank (EKB).

Availability of data and materials
The authors include all data generated or analyzed during the study in this published article and its supplementary information files. The datasets used and analyzed during the current study are available from the corresponding author upon reasonable request.

Declarations

Ethics approval and consent to participate
The authors declare their ethical approval and consent to participate.

Consent for publication
The authors declare consent for publication.

Competing interests
The authors declare that they have no competing interests. The authors declare that they have no known competing financial interests or personal relationships that could have appeared to influence the work reported in this paper.

Received: 8 June 2024 Accepted: 14 November 2024
Published online: 24 April 2025

References

Abdel Kareem, A. H. (2014). Shear strengthening of reinforced concrete beams with rectangular web openings by FRP composites. *Advanced Concrete Construction, 2*, 281–300. https://doi.org/10.12989/acc.2014.2.4.281

Abdel Kareem, A. H., Debaiky, A. S., Makhlouf, M. H., & Badwi, M. (2019). Repairing and strengthening RC beams using a thin lower concrete layer reinforced by FRP bars. *International Journal of Civil Engineering and Technology, 10*, 1949–66.

Abtan, Y. G. (2020). Structural behavior of fibrous SCC beams reinforced longitudinally by GFRP bars and strengthened with CFRP bonded at shear span. *Case Studies in Construction Materials*. https://doi.org/10.1016/j.cscm.2020.e00353

Al Saawani, M. A., El Sayed, A. K., & Al Negheimish, A. I. (2020). Effect of shear-span to depth ratio on debonding failures of FRP-strengthened RC beams. *Journal of Building Engineers, 32*, 101771. https://doi.org/10.1016/j.jobe.2020.101771

ANSYS 15 Manual Set, ANSYS Inc., South Pointe Technology Drive, FLEXLM License, Manager, Canonsburg, PA, U.S.A., 2015. (https://forum.ansys.com/uploads/846/SCJEU0NN8IHX.pdf).

ASTM International, Standard Test Method for Splitting Tensile Strength of Cylinder Concrete Specimens, ASTM C496–96 –(2015). (https://www.astm.org/c0496-96.html).

ASTM International: Standard Test Method for Compressive Strength of Cylindrical Concrete Specimens, ASTM C39/C39M-14, 2015. (https://www.studocu.com/row/document/state-engineering-university-of-armenia/concrete-design/astm-c39-c39m-14-concrete-design/32367366).

ASTM International, Standard Test Method for Static Modulus of Elasticity and Poisson's Ratio of Concrete in Compression, ASTM C469/C469M-14, West Conshohocken, 2021. (https://www.astm.org/c0469_c0469m-14.html)

B. S., Eurocode 2: design of concrete structures, Part 1–1: General rules and rules for buildings, European Committee for Standardization (CEN) (2004)1. https://www.phd.eng.br/wp-content/uploads/2015/12/en.1992.1.1.2004.pdf.

Ebrahim, E. A., Mahmoud, A. A., Salama, M. A., & Khater, A. N. M. (2024). Shear behavior of box-section concrete beams reinforced by FRP bars and FRP stirrups. *Structural Concrete Journal*. https://doi.org/10.1002/SUCO.202300129

ECP 208–2019. Egyptian Standing Code Committee for the Use of Fiber Reinforced Polymer (FRP) in Construction Fields. Housing and Building Research Center, Ministry of Building and Construction, Giza, Egypt, 2019. (https://www.studocu.com/row/document/jamaa%D8%A9-aayn-shms/concrete-structures-design/frp-egyptian-code-in-english/33457301).

Haddad, R. H., Al-Rousan, R. Z., & Al-Sedyiri, B. K. (2013). Repair of shear-deficient and sulfate-damaged reinforced concrete beams using FRP composites. *Engenering Structures, 56*, 228–238. https://doi.org/10.1016/j.engstruct.2013.05.007

Hassan, F. H., Medhlom, M. K., Ahmed, A. S., & Al-Dahlaki, M. H. (2020). Flexural performance of concrete beams reinforced by GFRP bars and strengthened by CFRP sheets. *Case Studies in Construction Materials, 13*, e00417. https://doi.org/10.1016/j.cscm.2020.e00417

Huang, Y., Lee, M. G., Kan, Y. C., Wang, W. C., Wang, Y. C., & Pan, W. B. (2022). Reinforced concrete beams retrofitted with UHPC or CFRP. *Case Studies in Construction Materials, 17*, 01507. https://doi.org/10.1016/j.cscm.2022.e01507

Masoud, M. R., & Khalaf, M. A. (2020). Effectiveness of shear and flexural repair and strengthening of box-section steel beams using CFRP laminates. *International Journal of Engineering and Advanced Technology, 2020*, 648–653. https://doi.org/10.35940/ijeat.C5335.029320

Muhammad, M. A., & Ahmed, F. R. (2023). Evaluation of deflection and flexural performance of reinforced concrete beams with glass fiber reinforced polymer bars. *Case Studies in Construction Materials, 18*(1), e01855. https://doi.org/10.1016/j.cscm.2023.e01855

Najaf, E., Orouji, M., & Ghouchani, K. (2022). Finite element analysis of the effect of type, number, and installation angle of FRP sheets on improving the flexural strength of concrete beams. *Case Studies in Construction Materials, 17*, e01670. https://doi.org/10.1016/j.cscm.2022.e01670

Nasser, M. A., Mahmoud, A. A., Mustafa, T. S., & Khater, A. N. M. (2024). Retrofitting of box-section concrete beams to resist shear and torsion using near-surface-mount (NSM) GFRP stirrups. *Frattura ed Integrità Strutturale, Fracture of Integrated Structure, 67*, 319–336.

Nassif, M. K., Erfan, A. M., Fadel, O. T., & El-Sayed, T. A. (2021). Flexural behavior of high-strength concrete deep beams reinforced with GFRP bars. *Case Studies in Construction Materials, 15*, e00613. https://doi.org/10.1016/j.cscm.2021.e00613

Nikopour, H., & Nehdi, M. (2011). Shear repair of RC beams using epoxy injection and hybrid external FRP. *Materials Structure Construction, 44*, 1865–1877. https://doi.org/10.1617/s11527-011-9743-8

Siddika, A., Mamun, M. A., Al, Y. R., & Amran, Y. H. M. (2019). Strengthening of reinforced concrete beams by using fiber-reinforced polymer composites: a review. *Journal of Building Engineers., 25*, 100798.

The American Code 440.2R-17: Guide for the Design and Construction of Externally Bonded FRP Systems for Strengthening Concrete Structures, 2017. (https://doi.org/10.14359/51700867).

Wei, B., He, X., Zhou, M., Wang, H., & He, J. (2024). Experimental study on flexural behaviors of FRP and steel bar hybrid reinforced concrete beams. *Case Studies in Construction Materials, 20*(12), e02759. https://doi.org/10.1016/j.cscm.2023.e02759

Zaher, A. H., Montaser, W. M., & Elsonbaty, M. M. (2020). Strengthening and repairing of RC deep beams using CFRP and GFRP. *International Journal of Civil Engineering and Technology, 11*, 64–85. https://doi.org/10.34218/ijciet.11.1.2020.008

Publisher's Note

Ahmed A. Mahmoud Professor of R.C. Structures, Civil Engineering Department, Faculty of Engineering (Shoubra), Benha University, Cairo, Egypt.

Manar S. Sedeek Research Assistant, Civil Engineering Department, Faculty of Engineering (Shoubra), Benha University, Cairo, Egypt.

Mohamed A. Salama Assistance Professor, Civil Engineering Department, Faculty of Engineering (Shoubra), Benha University, Cairo, Egypt

Ahmed N. M. Khater Assistance Professor, Civil Engineering Department, Faculty of Engineering (Shoubra), Benha University, Cairo, Egypt.